Apparent optical properties of oceanic water: dependence on the molecular scattering contribution

André Morel and Hubert Loisel

The relationships between the apparent optical properties (AOP's) and the inherent optical properties (IOP's) of oceanic water bodies have been reinvestigated by solution of the radiative transfer equation. This reexamination deals specifically with oceanic case 1 waters (those for which phytoplankton and their associated particles or substances control their inherent optical properties). In such waters, when the chlorophyll content is low enough (in most of the entire ocean), the influence of molecular scattering by water molecules is not negligible, leading to a gradual change in the shape of the phase function. The effect of this change on the AOP's is analyzed. The effect of the existence of diffuse sky radiation in addition to the direct solar radiation on AOP–IOP relationships is also examined. Practical parameterizations are proposed to predict in case 1 waters, and at various depths, the vertical attenuation coefficient for downward irradiance (K_d) as a function of the IOP's and solar angle. These parameterizations are valid for the spectral domain where inelastic scattering does not significantly occur (wavelengths below 590 nm).

OCIS codes: 010.0010, 010.4450, 290.4210.

1. Introduction

Solution of the direct problem of hydrologic optics is achievable through various methods (see the review in Ref. 1). This problem is simply formulated as follows: Given the constituents that determine the inherent optical properties (IOP's) of the water, and given the boundary conditions (the incident radiation field at the air–water interface for a deep ocean), compute the radiation field within the body of water. The progressive transformation of this field for increasing depth is described by various coefficients, collectively called apparent optical properties (AOP's). The distinction between the two mutually exclusive classes of properties (IOP's and AOP's) was made clear by Preisendorfer.[2] These two classes can be related through the radiative transfer equation, which, after mathematical manipulations, is explicitly used in analytical methods or is simulated by use of a probabilistic approach known as the forward Monte Carlo method. If the medium is deprived of internal sources, its IOP's reduce to the absorption coefficient a and the volume scattering function $\beta(\phi)$ (see definitions and symbols in Table 1).

The vertical attenuation coefficient for downward irradiance K_d, the subsurface irradiance reflectance R, and other AOP's have been studied, through Monte Carlo modeling, as a function of IOP's and the solar zenith angle.[3–7] Results (in terms of K_d and R) obtained for specific cases, treated as experimental data, were fitted to continuous empirical expressions that relate AOP's to IOP's, in which the coefficients depend on the Sun's position. In his previous studies, Kirk considered only one type of volume scattering function (VSF) and no sky light (as if the Sun were in a black sky). Later, Gordon[5] determined the extent to which such relationships (for R in particular) depend on the shape of the VSF. This problem was also reinvestigated by Kirk,[8] who made use of several specific VSF's determined by Petzold[9] in waters ranging from the clear oceanic type to coastal and turbid ones. As a result, the coefficients that appear in the empirical expressions were found to depend not only on the solar zenith angle but also on a descriptor of the VSF shape (the "average cosine of scattering," in Kirk's notation). The last-named study was also carried out under the assumption of a Sun in a black sky.

In oceanic case 1 waters[10,11] the variations in the shape of the VSF are not random. To first order they are governed by the respective proportions of molec-

The authors are with the Laboratoire de Physique et Chimie Marines, Université Pierre et Marie Curie and Centre National de la Recherche Scientifique, B.P. 08, F06238 Villefranche sur Mer Cedex, France.

Received 31 October 1997; revised manuscript received 12 March 1998.

0003-6935/98/214765-12$15.00/0

Table 1. Symbols Used

Symbol	Definition	Unit
a	Absorption coefficient	m^{-1}
b	Scattering coefficient	m^{-1}
b_w	Molecular scattering coefficient	m^{-1}
b_p	Particle scattering coefficient	m^{-1}
b_b	Backscattering coefficient	m^{-1}
$b_{b,p}$	Particle backscattering coefficient	m^{-1}
$\tilde{b}_{b,p}$	Particle backscattering probability ($=b_{b,p}/b_p$)	
$\beta(\phi)$	Volume scattering function	$m^{-1}\ sr^{-1}$
$\tilde{\beta}(\phi)$	Scattering phase function subscripts w and p for water molecules and suspended particles	sr^{-1}
[Chl]	Chlorophyll concentration	$mg\ m^{-3}$
g	Asymmetry parameter [Eq. (3)]	
c	Attenuation coefficient ($=a + b$)	m^{-1}
$\tilde{\omega}$	Single scattering albedo ($=b/c$)	
$\bar{n}$	Average number of collisions [$=1/(1-\tilde{\omega})$]	
η	Ratio of molecular scattering to total scattering	
θ	Solar zenith angle in air	
λ	Wavelength	nm
μ	Cosine of solar zenith angle in air	
μ_w	Cosine of solar zenith angle in water	
E_d, E_u	Downwelling and upwelling irradiance on a horizontal surface; subscripts d and u for downward and upward scalar irradiances, respectively	Wm^{-2}
E°	Total scalar irradiance	Wm^{-2}
R	Reflectance (irradiance ratio) ($=E_u/E_d$)	
$\bar{\mu}_d$	Mean cosine for downward flux ($=E_d/E_d^\circ$)	
$\bar{\mu}_u$	Mean cosine for upward flux ($=E_u/E_u^\circ$)	
K_d	Vertical attenuation coefficient [$=-d((\ln E_d)/dZ$]	m^{-1}
Z	Geometric depth	m
ζ	Optical depth ($=K_dZ$)	
τ_a, τ_r	Optical thickness that is due to aerosols (a) or to air molecules (r)	

ular scattering and of particle scattering, each with its specific VSF. These proportions, as well as the other IOP's (the absorption coefficient, in particular) are related to the locally formed biogenous materials, conveniently described by the chlorophyll concentration, denoted [Chl]. In oligotrophic oceanic waters with low [Chl] the importance of molecular scattering is definitely not negligible, especially in the blue part of spectrum (see Fig. 3 of Ref. 12). Indeed, the irradiance reflectance and the geometrical structure of upward radiance field just beneath the sea surface were found to be notably influenced by the contribution of molecular scattering and thus to vary according to the [Chl] value and the wavelength λ.[12,13] No doubt this influence extends to other AOP's in a way that remains to be examined.

Therefore the relationships between AOP's and IOP's are reinvestigated in a reasoned way, and the orderly evolution of IOP's with [Chl] in case 1 waters forms this logical guideline. At each wavelength the shape of $\beta(\phi)$ evolves in a regular manner as a result of the addition of a constant term that is due to molecules $\beta_w(\phi)$ and a variable term $\beta_p(\phi)$ that is due to particles; the magnitude of the latter is related to [Chl]. A preliminary and general study of the molecular scattering effect on the AOP's is presented and then realistic applications are envisaged. For practical purposes it is also necessary to quantify the effect of considering realistic incident radiative fields that include, besides the direct solar radiation, the diffuse sky radiation. As the inelastic processes are not accounted for, the practical applications of the present study are restricted to that spectral domain where the AOP's of the upper part of the water column are not significantly influenced by these processes. When λ exceeds 590 or 600 nm (see, e.g., Refs. 14 and 15) Raman scattering and chlorophyll fluorescence have a considerable effect on the light field, and this domain is not considered here.

2. Theoretical and Computational Considerations

In the present study the radiative transfer equation is solved by either the invariant embedding method (actually the Hydrolight 3.0 code[1]) or a Monte Carlo method.[12,13,16] The latter is used exclusively when the diffuse sky radiation has to be simulated with varying atmospheric conditions; in this case the Monte Carlo simulation encompasses both atmospheric and oceanic media. When operated for computing underwater light fields with the same input parameters and boundary conditions, the two codes provide perfectly coincident results, as has already been tested[16] and verified in the course of the present study.

For a given body of water the input parameters are dimensionless quantities derived from the IOP's, namely, (i) the scattering-to-absorption ratio b/a (see the notation defined in Table 1), (ii) the molecular-

scattering-to-total-scattering ratio $b_w/b = \eta$, where b, the total scattering coefficient, is the sum of molecular scattering and particle scattering, $b = b_w + b_p$, and (iii) the molecular scattering phase function $\beta_w(\phi)$ and the particle scattering phase function $\beta_p(\phi)$.

The b/a ratio was used extensively in Kirk's studies[6,7] and for the sake of comparison will be used hereafter. It is related to another ratio more commonly used in radiative transfer studies and known as the albedo for single scattering (or the probability of photon survival). It is defined as $\bar{\omega} = b/c$, where c is the attenuation coefficient ($c = a + b$), so

$$\bar{\omega} = \frac{(b/a)}{1 + (b/a)} \qquad \text{or} \qquad b/a = \frac{\bar{\omega}}{1 - \bar{\omega}}. \tag{1}$$

These relationships allow the results to be expressed as functions of either b/a or $\bar{\omega}$. The total scattering coefficient is expressed as

$$b = \int_{4\pi} \beta(\phi) \mathrm{d}\Omega,$$

and the volume scattering function $\beta(\phi)$ [$\mathrm{m}^{-1}\ \mathrm{sr}^{-1}$] is related to the phase function $\bar{\beta}(\phi)$ [sr^{-1}] through

$$\beta(\phi) = b\bar{\beta}(\phi).$$

The scattering phase function $\bar{\beta}(\phi)$ of a water body with a prescribed η value is expressed as the weighted sum of the two phase functions for molecules and particles with subscripts w and p, respectively:

$$\bar{\beta}(\phi) = \eta\bar{\beta}_w(\phi) + (1 - \eta)\bar{\beta}_p(\phi). \tag{2}$$

The shapes of these two phase functions differ sharply (see Fig. 1). The overall shape is conveniently described by the asymmetry parameter (called the average cosine of scattering by Kirk[8]), defined as

$$g = \int_{4\pi} \bar{\beta}(\phi)\cos(\phi)\mathrm{d}\Omega. \tag{3}$$

For the symmetrical phase function of water molecules $g_w = 0$, whereas g_p is close to 1 for the scattering function highly peaked in the forward direction that is typical of suspended marine particles. In the present study a unique particle phase function for particles is used, which was proposed by Mobley *et al.*[16] (see Table 3.10 of Ref. 1). This function was derived by averaging of three particle phase functions determined in oceanic waters by Petzold.[9] The asymmetry parameter for this function is 0.924, so as a consequence of Eqs. (2) and (3) the asymmetry for a given oceanic water, g, is expressed as

$$g = \eta g_w + (1 - \eta)g_p = (1 - \eta)0.924. \tag{4}$$

This relationship obviously stresses that g, the descriptor of the shape of the phase function, is univocally related to η. It is a straightforward consequence of our having adopted a unique phase function for suspended particles, and this limitation is discussed below.

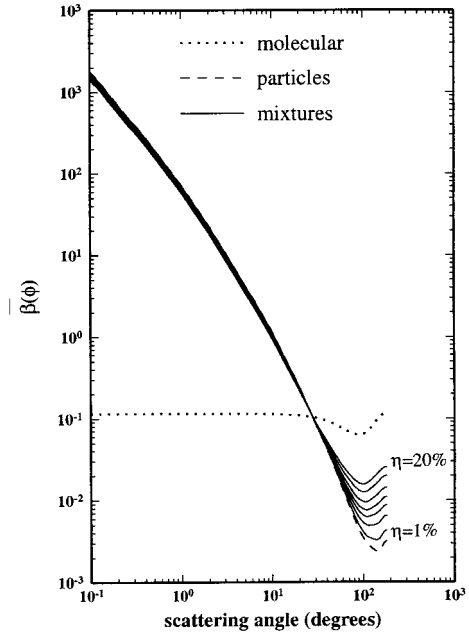

Fig. 1. Phase functions for molecular scattering, for particles, and for mixtures [Eq. (2)] with variable η values in percent (1, 3, 5, 7, 10, 15 and 20 from bottom to top).

Geometric depths within the water column, and thus vertical discretization in the computation, are determined as soon as one of the IOP's above is given an absolute value; in the present simulations the absorption coefficient a is set equal to 1 m^{-1}. Such an arbitrary choice in no way affects the general character of the results, to the extent that the outputs (like inputs) are also presented and discussed in terms of dimensionless quantities. These quantities are K_d/a, the ratio of the attenuation coefficient for downwelling irradiance to the absorption coefficient, the irradiance reflectance R, and the average cosines for the downward and upward radiant field μ_d and μ_u, respectively (see Table 1). They are studied as functions of b/a and η and for various Sun angle and atmospheric conditions (various aerosol loads in cloudless atmospheres). Their localized values are examined at different optical depths ζ, defined as

$$\zeta = K_d Z, \tag{5}$$

where Z is the geometrical depth so ζ is dimensionless. Averaged values of K_d/a are also computed for layers extending from 0 to a given ζ value; in such cases they are denoted $\langle K_d/a\rangle_{\Delta\zeta=\zeta}$. All computations deal with homogeneous waters, with IOP's uniformly distributed along the vertical. Even in such bodies of water, K_d varies with depth, so ζ is not strictly proportional to Z. In contrast, the optical thickness τ ($=cZ$) that involves an IOP has a more universal meaning. In the present study, however, ζ ($=\tau K_d/c$) is preferred because it is closely related to field studies

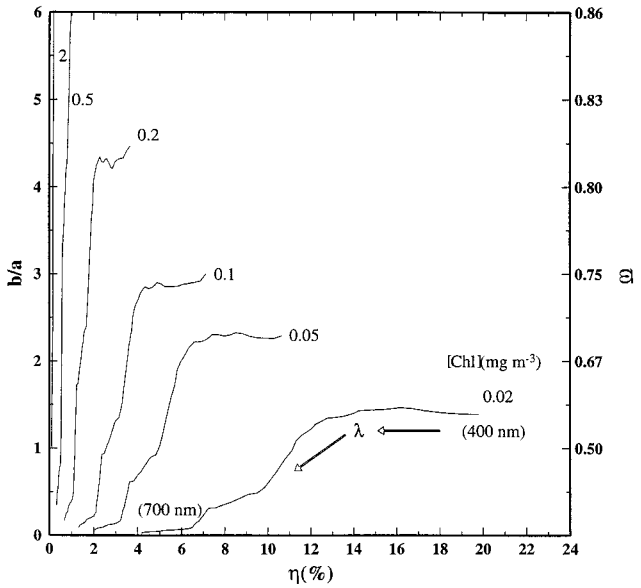

Fig. 2. Variations of b/a (and $\bar{\omega}$, right-hand scale) with η within the 400–700-nm spectral domain and for various [Chl] values from 0.02 to 2 mg m^{-3}, as indicated.

and defines in a convenient way the levels where given fractions of incident downward radiation still remain.

The IOP's of oceanic case 1 waters[10] are modeled as a function of [Chl] as previously made[12]:

$$b(\lambda) = b_w(\lambda) + (550/\lambda)0.3[\mathrm{Chl}]^{0.62}, \quad (6)$$

$$a(\lambda) = [a_w(\lambda) + 0.06A(\lambda)[\mathrm{Chl}]^{0.65}][1 + 0.2Y(\lambda)], \quad (7)$$

where the first bracketed term in Eq. (7) contains the normalized specific absorption of phytoplankton, $A(\lambda)$, and the second bracketed term expresses the contribution to absorption of a locally formed yellow substance.[17] The spectral dependency of yellow substance absorption is modeled according to Bricaud *et al.*[18] as

$$Y(\lambda) = \exp[-0.014(\lambda - 440)].$$

The two dimensionless quantities (b/a and η) used as descriptors of any body of water are straightforwardly derived from Eqs. (6) and (7) as functions of λ and [Chl]. According to the wavelength and the [Chl], b/a can vary from 0.05 ($\bar{\omega} < 0.05$) to ~6 ($\bar{\omega} \simeq 0.85$), and η from 0 to ~20% (see Figs. 2 and 3 of Ref. 12). Higher η values can occur in the near-UV domain (not considered here). As a consequence of our having assumed a regular evolution of IOP's with [Chl] in Case 1 waters, these two parameters do not vary independently. Their concomitant variations [derived from Eqs. (6) and (7)] within the 400–700-nm spectral domain and for various [Chl] values are shown in Fig. 2. This figure puts in evidence a forbidden domain that corresponds to unrealistic $b/a - \eta$ combinations (for case 1 waters); for example, high η values do not coexist with high b/a values. These limitations have to be borne in mind even if a wider domain is considered in the following, more general, computations.

Another limitation arises from the adoption of a unique phase function for suspended particles. Assuming that the shape of this function is invariable is unrealistic when the whole [Chl] range is considered. In particular, with the adopted function the backscattering probability ($\tilde{b}_{b,p} = 0.019$) is definitely too high when [Chl] exceeds 2 or 3 mg m^{-3} (see Fig. 4 of Ref. 12) and thus affects the validity of the results for those AOP's (μ_u and R) that are more influenced by the backscattering properties. A better knowledge of the scattering phase function of hydrosols is not yet available and is definitely needed for further improvements.

The atmosphere is modeled with 50 1-km-thick layers (from 0 to 50 km); specified values for Rayleigh and aerosol scattering and for ozone absorption[19] are prescribed for each layer. Aerosols of a rural type with a relative humidity of 70% are present within the 45 upper layers (from 5 to 50 km). The corresponding optical thickness (at 550 nm), $\tau_a(5\text{–}50) = 0.0493$, is kept constant. Aerosols of the maritime type with a relative humidity of 90% are located within the five lower layers; the corresponding optical thickness, $\tau_a(0\text{–}5)$, is made to vary in such a way that the total aerosol optical thickness $\tau_a = \tau_a(0\text{–}5) + \tau_a(5\text{–}50)$ varies from 0.10 to 0.80 (always at 550 nm); these values roughly correspond to horizontal visibilities of 40 and 5 km, respectively. The models for these aerosols were taken from Shettle and Fenn,[20] and their phase functions were computed through Mie theory for the various wavelengths of interest. The optical thickness for air molecules is $\tau_R(550) = 0.098$ and varies spectrally according to $\lambda^{-4.09}$. The air–sea interface is modeled following Cox and Munk[21]; for the present computations the wind speed was set equal to zero, and in the absence of wind, only residual capillary waves were present.

Beside the possibility of cross checking offered by simultaneously operating two codes, an internal control was systematically made; it consisted in verifying that the absorption coefficient used as input (1 m^{-1}) is retrieved from (four) computed quantities according to

$$a = \frac{K_d}{1/\bar{\mu}_d + R/\bar{\mu}_u}\left(1 - R + \frac{1}{K_d}\frac{\mathrm{d}R}{\mathrm{d}z}\right), \quad (8)$$

which is an exact relationship directly derived from Gershun's equation (divergence law for irradiance). The a value was always retrieved with an accuracy of better than 0.3%.

3. Results

For a direct comparison with Kirk's results the diffuse sky radiation is not simulated in the first series of computations discussed below, and the wavelength is not specified. The presentation of the results is made in order of optical depths. Emphasis is put on the variations in AOP's that originate from the variable influence of molecular scattering. The second series

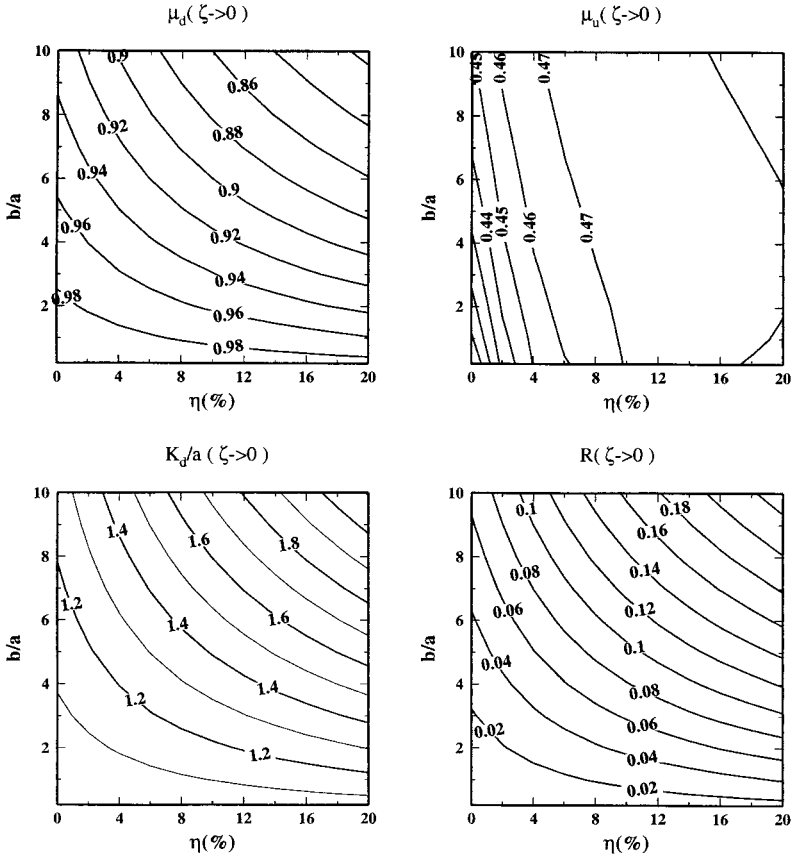

Fig. 3. In the $b/a - \eta$ plane, isopleths of the AOP beneath the air–water interface ($\zeta = 0$) for the Sun at zenith (and in a black sky).

of computations simulates realistic situations including the sky radiation and deals with typical examples of oceanic waters in terms of wavelength and [Chl]. As in previous studies,[4,5,7,12] the AOP's that result from all numerical simulations are treated as experimental data and are fitted to empirical polynomials in which the coefficients are made explicit functions of the relevant parameters (η and μ_w).

A. Radiative Regime beneath the Air–Water Interface ($\zeta \to 0$)

Apart from $\bar{\mu}_u$, which involves only the upward flux and thus has a clear meaning at $\zeta = 0$, the other AOP's (K_d/a, $\bar{\mu}_d$, and R) have to be considered in their limit values when ζ tends toward 0. In practice, the computations were made with $\zeta = 0.01$. The first results presented are for vertically incident light ($\theta = 0$). The localized AOP values are shown in Fig. 3 as isolines drawn within the $b/a - \eta$ plane. Additional information is provided in Table 2, where the influence of accounting for an increasing proportion of molecular scattering is quantified as

$$\delta(\mathrm{AOP}) = \frac{\mathrm{AOP}(\eta = 20\%) - \mathrm{AOP}(\eta = 0\%)}{\mathrm{AOP}(\eta = 0\%)}. \quad (9)$$

The behavior of R just beneath the surface has already been thoroughly analyzed,[12] and only brief comments are needed here. To the extent that R is related to the ratio b_b/a, it regularly increases along with b/a, albeit in a nonlinear manner as b_b/b is not constant and actually depends on η. When η increases, the relative increase of $\tilde{\beta}(\phi)$ for the backward directions ($\phi > \pi/2$; see Fig. 1) results in a global heightening of the ratio b_b/b and thus of R. This effect is particularly pronounced when the upward flux is made up predominantly of photons that have experienced (on average) a reduced number of scattering events (e.g., $\bar{n} = 1.2$; Table 2); it is reduced when the diffuseness of the light regime is progressively set up by multiple scattering (increasing $\bar{n}$). The mean cosine for upward flux, $\bar{\mu}_u$, is weakly dependent on b/a, increases rather regularly with η, and reaches a value (0.48 when η is 20%) not far from that which describes a perfectly isotropic upward radiance field (0.50). The mean cosine for downward flux, $\bar{\mu}_d$, departs from 1 (the value for a purely absorbing medium) as soon as b/a departs from 0, and for a given b/a value the departure is slightly enhanced when the influence of molecular scattering is rising. This effect is obviously related to the lowering of the asymmetry parameter, which decreases from 0.924 to 0.739 when η increases from 0 to 20% [Eq. (3)].

As soon as scattering occurs, K_d/a is superior to 1 and the relative contribution of scattering to vertical attenuation of irradiance can be conveniently expressed as proposed by Kirk[6,7] through an empirical simple equation

$$K_d/a = {\mu_w}^{-1}\left[1 + G(\mu_w)\frac{b}{a}\right]^{1/2}, \quad (10)$$

Table 2. Changes (in %) in μ_u, μ_d, K_d/a, and R When η Decreases from 20 to 0% [Eq. (9)] and for Selected b/a Values at Various ζ Values or for $\Delta\zeta = 1$ as Indicated[a]

b/a	$\bar{\omega} = b/c$	$\bar{n}$	δ_{μ_u}	δ_{μ_d}	$\delta_{K_d/a}$	δ_R
$\zeta = 0$						
0.2	0.17	1.2	20.8	−0.56	2.5	606
1.0	0.5	2	18.3	−2.6	11.6	545
5.0	0.83	6	11.1	−8.8	44.3	363
10	0.91	11	7.2	−12.3	68	259
$\zeta = 1$						
0.2	0.17	1.2	21.5	−0.92	2.77	599
1.0	0.5	2	21.3	−3.4	12.5	515
5.0	0.83	6	18.5	−7.3	40.6	294
10	0.91	11	15.4	−7.6	55.1	194
$\zeta = 2.3$						
0.2	0.17	1.2	21.1	−1.64	3.83	602
1.0	0.5	2	22.6	−3.44	12.5	496
5.0	0.83	6	20.8	−6.3	38.5	268
10	0.91	11	17.9	−6.4	52.1	179
$\zeta = \infty$						
0.2	0.17	1.2	23.4	−0.74	2.7	700
1.0	0.5	2	25	−3.4	12.4	457
5.0	0.83	6	21.4	−6.3	38	245
10	0.91	11	16.7	−6.38	52.3	161
$\Delta\zeta = 1$						
0.2	0.17	1.2	21.2	−0.74	2.5	602
1.0	0.5	2	19.9	−3.1	12.2	528
5.0	0.83	6	15.2	−8.0	41.1	321
10	0.91	11	11.8	−9.6	60.7	222

[a]For $\zeta = \infty$ the asymptotic regime was computed as in Ref. 22.

where G is a coefficient that depends on μ_w, the cosine of the refracted solar rays just beneath the surface. This approximate relationship is verified in the present case to involve various η values. A separate regression, restricted to the data with $\mu_w = 1$, demonstrates that G can be related (with $r^2 = 0.99$) to η through a simple linear expression:

$$G(\mu_w = 1, \zeta = 0) = 0.0527 + 1.371\eta. \quad (11)$$

For a given b/a value the departure of K_d/a from 1 increases when the scattering is less concentrated within the forward direction (i.e., when η is higher and g is less). The effect of increasing the molecular scattering contribution is also clearly seen in Fig. 4 (similar to Fig. 1 of Ref. 8).

When the incident light is no longer vertical and the solar zenith angle is progressively increasing, $\bar{\mu}_d$ and $\bar{\mu}_u$ decrease (not shown), whereas K_d/a and R are increasing. To account for the dependence of K_d/a on the Sun's angle, we can now fit the G coefficient ($r^2 = 0.96$) to an expression involving both η and μ_w, which is written as

$$G(\mu_w, \zeta = 0) = (0.131 + 1.039\eta) + (-0.077 + 0.344\eta)\mu_w. \quad (12)$$

Note that Eq. (12), operated with $\mu_w = 1$, coincides with Eq. (11) within ~2%.

The K_d coefficient just beneath the surface was also studied by Gordon[4] and was related [his Eq. (10)] to a and b_b, the backscattering coefficient, through

$$K_d = (\mu_w)^{-1}\, 1.0395(a + b_b). \quad (13)$$

By recalling that for the particle phase function used here $\tilde{b}_{b,p} = 0.019$ and that $\tilde{b}_{b,w} = 0.5$, we can express b_b as a function of b and η [in the same way as for β in Eq. (2)], so Eq. (13) can be rewritten as

$$K_d/a = (\mu_w)^{-1}\, 1.0395\left[1 + \frac{b}{a}(0.481 - 0.019\eta)\right]. \quad (14)$$

The present numerical results satisfy Eq. (14) within ±3% (if $\theta < 60°$ and $b/a < 6$). Note that the average cosine in Gordon's expression accounts for the presence of the atmosphere, whereas the present calculations ignore the sky radiation (so that μ_w is controlled only by the Sun's angle).

The variations in R at null depth with the solar angle, and when the contribution of the molecular scattering is changing, were analyzed previously. Practical formulas can be found in Ref. 12, when $\bar{\omega} < 0.80$ ($b/a < 4$), that are valid for most oceanic waters; more comprehensive formulas that also include the dependence on $\bar{\omega}$ (which are more accurate when $\bar{\omega} \geq 0.80$) were proposed by Morel and Gentili.[13] The formulas were established in realistic illumination conditions (Sun plus sky) and are not discussed further here.

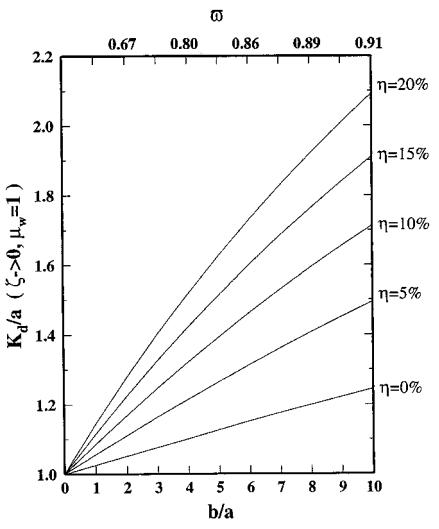

Fig. 4. K_d/a beneath the air–water interface for a Sun at zenith as a function of b/a (and $\bar{\omega}$) for various η values.

B. Radiative Regime within the Upper Layer (at $\zeta = 1, 2.3$)

As was demonstrated by Gordon and McCluney,[3] ~90% of the photons that form the upward flux just beneath the surface originate from the layer located between $\zeta = 0$ and $\zeta = 1$. This layer accordingly is of particular interest in remote-sensing applications. For this layer, average values of the ratio $\langle K_d/a \rangle_{\Delta\zeta=1}$ were given by Kirk[8] and related to the shape of the phase function. Localized values of K_d/a at $\zeta = 2.3$

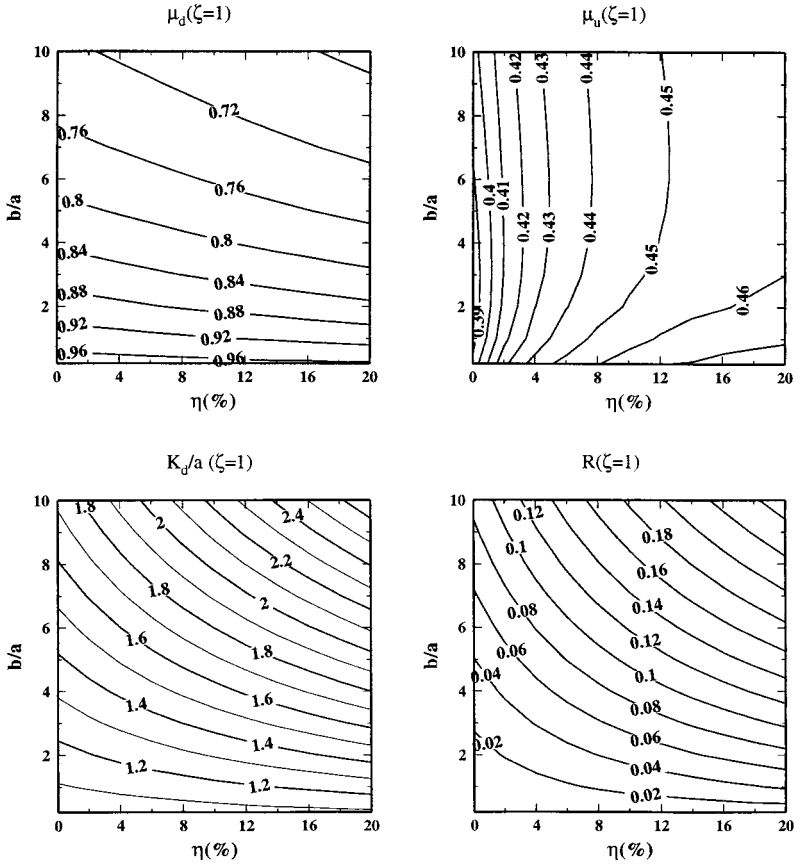

Fig. 5. As in Fig. 3 but at the first attenuation depth ($\zeta = 1$).

were also computed[7] under the assumption of a unique phase function (that of San Diego Harbor, determined by Petzold[9]). The dimensionless AOP's were computed for $\zeta = 1, 2.3$. The results for $\zeta = 2.3$, and when $\theta = 0$, are displayed in Fig. 5, which is similar to Fig. 3. Compared with the subsurface situation, the radiative regime is progressively more diffuse and the downward flux less concentrated toward the nadir (light is vertically incident). All the $\bar{\mu}_d$ values (in the b/a, η plane) are significantly lower, and correlatively all the K_d/a values exceed those at the subsurface. As expected, the average cosine $\bar{\mu}_u$ changes less and essentially remains governed by the η values (except in low b/a conditions). With increasing ζ, the overall pattern of the R isopleths is unchanged, whereas the R values themselves are increasing. The relative changes (positive or negative) in each of the AOP's, expressed as

$$\epsilon = \frac{\mathrm{AOP}(\zeta = 2.3) - \mathrm{AOP}(\zeta = 0)}{\mathrm{AOP}(\zeta = 0)}, \qquad (15)$$

are displayed in Fig. 6 for two selected cases ($\eta = 5\%$ and b/a varying, or $b/a = 5$ and η varying). In brief, although the AOP's are evolving along with depth, their dependence on η does not vanish. Actually this dependency persists even in the asymptotic ($\zeta = \infty$) diffuse regime (see Table 2).

A first comparison is possible at $\zeta = 2.3$ with the results published by Kirk,[7] who expressed the factor $G(\mu_w, \zeta = 2.3)$ as

$$G(\mu_w, \zeta = 2.3) = 0.473\mu_w - 0.218. \qquad (16)$$

When they are fitted ($r^2 = 0.98$) to an expression that has the same structure, the present data lead to

$$G(\mu_w, \zeta = 2.3) = (0.451 + 2.584\eta)\mu_w - (0.2046 + 0.521\eta). \qquad (17)$$

Equation (17) accounts for the influence of η in modifying the two coefficients of Eq. (16). When η is set equal to 0, only minute differences occur between the results produced by the two equations [Fig. 7(a)]. Equation (17) actually leads to values below those that result from Eq. (16) by 2–3.5%, likely as a consequence of use of two slightly different particle phase functions. In contrast, as soon as η is not 0, considerable differences appear; for instance, $G(\mu_w, \zeta = 2.3)$ is multiplied by approximately a factor of 3 [Fig. 7(a)] when η varies from 0 to 20% and for all solar angles. The consequences of this change in G for K_d/a are shown in Fig. 7(b) for the particular instance of a zenith Sun angle (in air) equal to 30° (recall that the domain with simultaneous high b/a and η values is unrealistic).

The average values $\langle K_d/a \rangle_{\Delta\zeta=1}$ within the first at-

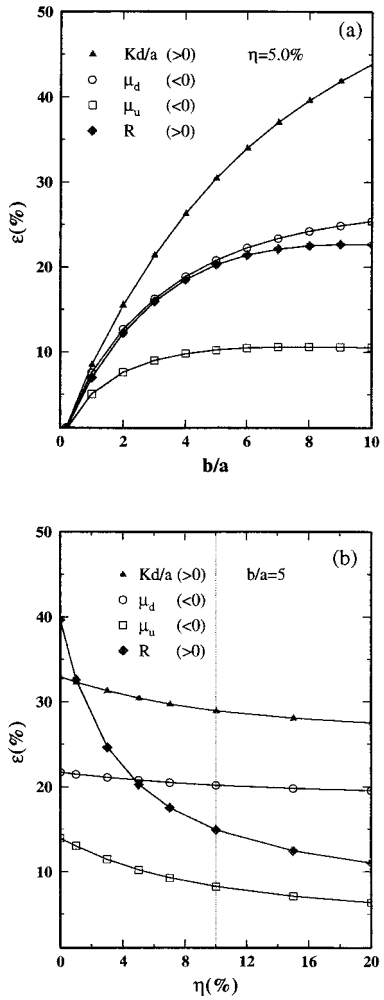

Fig. 6. (a) Relative change of the AOP over the interval $\zeta = 0$ and $\zeta = 2.3$ for a Sun at zenith and $\eta = 5\%$ as a function of b/a. Data are computed through Eq. (15). (b) As in (a) but for η varying and $b/a = 5$.

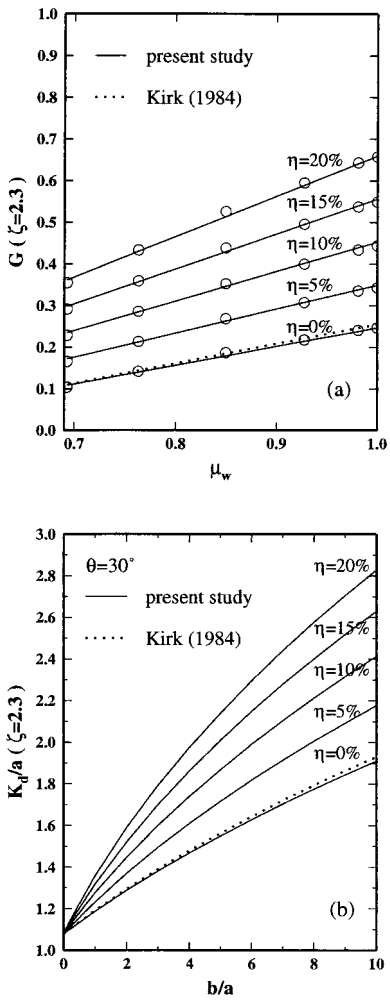

Fig. 7. (a) Variations of G with μ_w, the cosine of the Sun's zenith angle after refraction, for several η values: open symbols, results of computations; curves, calculated from Eq. (17). (b) K_d/a as function of b/a at $\zeta = 2.3$ with a light incident at 30°. Solid curves, computed according to Eq. (17); dashed curves (Kirk's result), according to Eq. (16).

tenuation layer have also been computed and fitted in the same way as above, on

$$G(\mu_w, \Delta\zeta = 1) = (0.1304 + 0.272\eta) + (-0.01414 + 1.343\eta)\mu_w. \quad (18)$$

A comparison with Kirk's results is possible only for $\mu_w = 1$ (see Table 3). Kirk's results deal with diverse phase functions, actually with diversified waters. Between the two sets of $G(\mu_w = 1, \Delta\zeta = 1)$ values we establish the link by relating the asymmetry values indicated by Kirk to the η values [with Eq. (4)]. There is a limitation in such a comparison because some of the waters considered by Kirk (namely, waters 5 and 6; Southern California) exhibit a g value (0.947) that is already above the upper limit ($g_p = 0.924$) that corresponds to the particle phase function now used. For the other waters, however, and when g varies between 0.922 and 0.885 (corresponding to η values from 0.2% to 4.2%), close agreement can be observed between Kirk's values and the G values produced by Eq. (16). Equation (16), in addition, allows the influence of the solar angle to be accounted for. It will be modified below to include the effect of diffuse sky radiation in addition to the direct solar radiation.

C. Influence of the Diffuse Sky Radiation on the Apparent Optical Properties

In the above simulations, all performed with a Sun in a black sky, the wavelength was never specified and the input parameters b/a and η were allowed to be

Table 3. G Values for the Layer of Optical Thickness $\Delta\zeta = 1$ for $\mu_w = 1$

g	η (%)	G^{Kirk}	G	Deviation (%)[a]
0.922	0.216	0.126	0.1198	5.17
0.915	0.974	0.137	0.1320	3.80
0.867	6.169	0.216	0.2160	0
0.885	4.220	0.186	0.1845	0.81

[a] $(G^{\text{Kirk}} - G)/G$.

free, independently varying, parameters (but see Fig. 2). Adding diffuse incident radiation to those previous simulations would be meaningless from a practical viewpoint. Indeed, for a given Sun elevation the relative importance of diffuse and direct radiation in forming the incident flux at the surface is highly dependent on the wavelength. At this stage it becomes necessary to fix the conditions in a realistic way. We must define the wavelength to derive the appropriate b/a and η values [through Eqs. (6) and (7)], and the atmospheric properties (the aerosol load in particular) have to be selected. The simulations thus involve both the atmosphere and the ocean.

The wavelengths particularly considered here (namely, 410, 443, 490, 560, and 665 nm) are those often used for the ocean color studies. The [Chl] range begins at 0.02 mg m^{-3} and, for reasons already explained, is limited to 2 mg m^{-3}. The aerosol optical thickness (τ_a at 550 nm) varies from 0.10 to 0.80. For practical purposes the analysis of the results is focused mainly on two particular oceanic layers, from the surface to the first attenuation depth ($\zeta = 1$) and to the level where the incident flux is reduced to 1% of its initial value (at $\zeta = 4.6$). To the extent that the reflectance beneath and above the interface as well as the bidirectional properties of the radiance field emerging from the sea were previously studied in similar realistic conditions,[12,13,23] the examination below deals essentially with the behavior of K_d/a.

The overall effect of accounting, at null depth, for the contribution of a diffuse component to the total solar incident flux can be seen in Fig. 8 for a particular instance with $\lambda = 445$ nm and [Chl] = 0.10 mg m^{-3}. As expected, the variations with Sun angle of all AOP's are smoothed by the addition of diffuse radiation. At the wavelength considered, the Rayleigh scattering is important, and τ_R, the corresponding optical thickness that is due to air molecules, is ~0.238. Therefore the departure of the AOP's from their values for a Sun in a black sky is notable, even for τ_a as small as 0.1. Within the red part of the spectrum, at 665 nm for instance, where τ_R is reduced to 0.0453, the changes in the AOP's, which are essentially governed by τ_a, thus increase more regularly with τ_a (see Fig. 8 for K_d/a only). The departures generated by the diffuse radiation are maximal at $\theta = 0°$ and are again noticeable for $\theta > 60°$. Between these values of θ there is an angular domain (centered around 50°) where $\cos(\theta)$ and the average cosine for the downward sky radiation cross each other, which results in AOP's becoming practically insensitive to the sky radiation.

The average $\langle K_d/a \rangle_{\Delta\zeta}$ value for the $\Delta\zeta = 4.6$ layer was parameterized by Kirk[7] according to

$$\langle K_d/a \rangle_{4.6} = (\mu_w)^{-1}\left[1 + (0.425\mu_w - 0.190)\frac{b}{a}\right]^{1/2}. \quad (19)$$

The values predicted from Eq. (19) for $\theta = 0$ and the present results are compared in Fig. 9. Kirk's formula is used with the appropriate b/a values for the wavelengths and [Chl] considered. The present

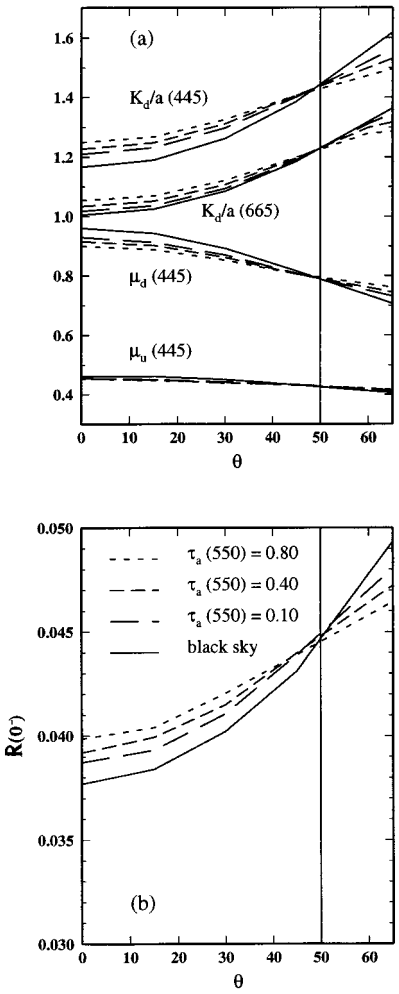

Fig. 8. (a) Evolution of K_d/a, $\bar{\mu}_d$, and $\bar{\mu}_u$ beneath the sea surface ($\zeta = 0$) at the wavelength 445 nm and with a [Chl] of 0.1 mg m^{-3} as functions of the Sun's zenith angle θ and for several aerosol optical thicknesses $\tau_a(550)$. For comparison, the value of K_d/a at 665 nm is also shown (note that K_d is not influenced by Raman scattering at the depth considered). (b) Evolution of the reflectance beneath the sea surface for a [Chl] of 0.1 mg m^{-3} at 445 nm as a function of θ and for various $\tau_a(550)$ values.

computations account, in addition, for the changing η value (with [Chl] and λ; Fig. 2) and for the effect of sky radiation [depending on $\tau_r(\lambda)$ and $\tau_a(\lambda)$].[24] To discriminate between the two effects, we also performed simulations without sky radiation; in this case the deviations (with respect to the Kirk's values) are due exclusively to the effect of molecular scattering via η (see the curves labeled black sky in Fig. 10).

There are considerable differences between the two sets of data. As expected, the deviations from Kirk's predictions are striking for shorter wavelengths and lower [Chl]. The relative deviations (expressed in percent) are shown in Fig. 10. If we disregard the results for 560 nm, for which the relative differences actually are minute, the results for the other wavelengths deserve three main observations:

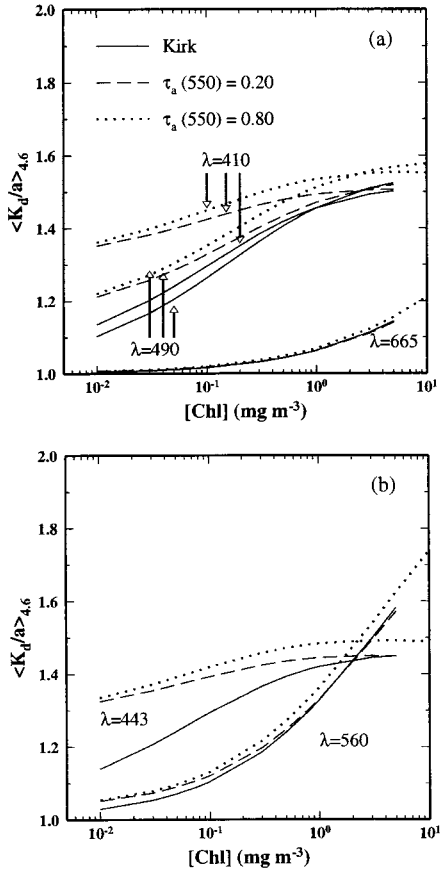

Fig. 9. $\langle K_d/a\rangle_{4.6}$ averaged over $\Delta\zeta = 4.6$ and for selected wavelengths (in nanometers) as indicated, as a function of [Chl] when the Sun is at zenith. Solid curves, K_d/a values computed through Eq. (19) (Kirk's expression); dashed and dotted curves, K_d/a derived from Eqs. (20) and (21), and by use of the coefficients for a real sky ($\Delta\zeta = 4.6$, Table 4).

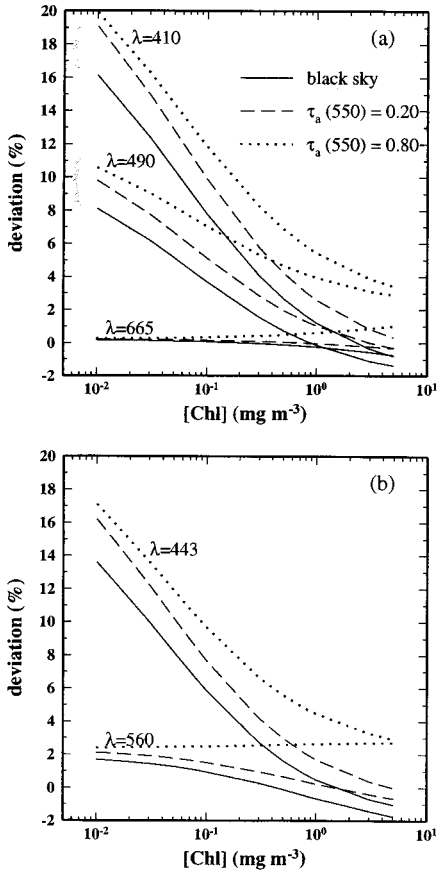

Fig. 10. Relative deviations (expressed as percent) between the present results [Eqs. (20) and (21)] and Kirk's result [Eq. (19)] for selected wavelengths and various sky conditions, plotted as a function of [Chl].

(i) For the blue radiation (from 410 to 490 nm) the effect of molecular scattering in forming the deviations is preponderant for low [Chl] and extends to [Chl] values to ~1 mg m^{-3}; the deviations are reinforced by the introduction of diffuse sky radiation.

(ii) For [Chl] > 1 mg m^{-3}, η is vanishingly small, and the deviations are essentially due to the sky radiation.

(iii) Overall, for most oceanic waters characterized by low [Chl] (Refs. 25 and 26) and as a consequence exhibiting a high transparency for blue radiation (λ < 500 nm), the deviations are important (5–20%) and are worthy of being considered when one is modeling the optical properties of the euphotic layer.

For other solar angles (results not shown), patterns similar to those in Fig. 9 are obtained. As a consequence of the existence of a hinge point in Fig. 8, the deviations with regard to Kirk's formula reduce to those that originate from the sole influence of η when θ is ~50°.

From the same series of simulations the $\langle K_d/a\rangle$ values for the upper layer ($\Delta\zeta = 1$) have been computed. For given λ and [Chl] these values are always less by approximately 10–15% than those for the $\Delta\zeta = 4.6$ layer. There are no published data with which they can be compared.

All the above data can be fitted and then represented according to the general formula

$$\langle K_d/a\rangle_{\Delta\zeta} = (\mu_w)^{-1}\left(1 + \Gamma\frac{b}{a}\right)^{1/2}, \qquad (20)$$

Table 4. Values for the Four Coefficients of Eq. (21)[a]

Sky	Black	$\tau_a(550) = 0.2$	$\tau_a(550) = 0.8$
$\Delta\zeta = 1$			
γ_1	+0.1304	0.00054	−0.11537
γ_2	0.272	−0.3005	−1.286
γ_3	−0.01414	0.1183	0.27899
γ_4	1.3433	2.0303	3.063
r^2	0.98	0.97	0.97
$\Delta\zeta = 4.6$			
γ_1	−0.1538	−0.2227	−0.3781
γ_2	0.22475	−1.8338	−1.407
γ_3	0.3714	0.44815	0.6304
γ_4	1.467	3.8135	3.357
r^2	0.98	0.99	0.98

[a]See text; $r^2$are the determination coefficients.

where

$$\Gamma(\Delta\zeta, \tau_a) = (\gamma_1 + \gamma_2\eta) + (\gamma_3 + \gamma_4\eta)\mu_w. \quad (21)$$

The Γ coefficient depends on η and μ_w through four coefficients (γ_1, γ_2, γ_3, γ_4); in turn, these coefficients depend on the layer considered, say, $\Delta\zeta = 1$ or $\Delta\zeta = 4.6$, and on the atmospheric properties through $\tau_a(550)$. The corresponding coefficients are provided in Table 4. In addition, those for a Sun in a black sky are given for comparison. At least when $0.1 < \tau_a(550) < 0.4$, the $\langle K_d/a \rangle$ values (for $\Delta\zeta = 1$ or $\Delta\zeta = 4.6$) are weakly changing (actually by less than 1.5%); therefore the intermediate values [corresponding to $\tau_a(550) = 0.2$] can be safely adopted in most situations.

4. Conclusions

As was already shown for reflectance,[12] the other AOP's of oceanic case 1 waters distinctly depend on the respective contributions of molecular scattering and particle scattering. The influence of the former, through the change in the shape of the phase function, is particularly clear when one examines the behavior of the K_d/a ratio, and this effect is expected to occur in most parts of the world ocean. Indeed, oligotrophic regimes with low [Chl] predominate (see, e.g., Refs. 25 and 26). In such situations the particle content is at its minimum and thus leads to high η values, particularly in the short-wavelength domain, which is of particular interest in these blue waters. Whatever the optical depth considered, K_d/a is always superior when the molecular scattering interferes, compared with its value when scattering is caused only by suspended particles.

Taking into account the existence of diffuse sky radiation (beside the direct solar flux) has a lesser effect than molecular scattering in modifying the relationships between IOP's and AOP's. Nevertheless, the effect is in the same direction, so K_d/a is again increased when the sky radiation is considered as well as when this diffuse radiation is rendered more intense by an increase in the atmospheric turbidity.

When the presentation is made as a function of [Chl] and wavelength (Figs. 9 and 10), the results depend on the way the AOP is modeled for Case 1 waters [Eqs. (6) and (7)]. The parameterizations as proposed, however, do not depend on the model, for they rely only on the η and b/a values (Table 4). It is likely that improved models will be developed that will lead to modified relationships between $\eta(\lambda)$ or $b/a(\lambda)$ and [Chl]. Such changes will not preclude the use of the present parameterizations. If in future models the possible variations in the particle phase function with [Chl] can be represented (as desirable), further computations, or at least sensitivity studies with respect to these variations, will be necessary.

Emphasis has been put on the euphotic layer and on the upper layer corresponding to the first attenuation depth. When the primary production is modeled (see, e.g., Ref. 12), at least the entire euphotic layer must be considered, and the irradiance that is involved is the scalar irradiance, E°. Most of the past measurements and bio-optical models[27–29] actually have dealt with E_d. The ratio K_d/a numerically expresses (in fact overestimates by only a few percent) the ratio E°/E_d, so one can directly use the proposed parameterization to perform the needed conversion. Note that in the same series of computations E° and all the other AOP's (the vertical attenuation coefficient for the upward and total irradiances and the mean cosine for the entire field) have been obtained, and these results are available from the authors on request. The specific formulas for $\zeta = 1$ are intended to provide a tool for modeling the optics of the layer seen by a remote sensor. The relationships between AOP's and IOP's change rapidly in the vicinity of the interface, so bulk relationships that are valid for thicker layers are not adapted when we describe the upper layer, and specific relationships are to be preferred.

This research was supported principally by the Agence Spatiale Européenne (contract 11.878/96/NL/GS). We thank B. Gentili for his continual help in computational problems. Recognition and thanks are given to an anonymous reviewer for a critique of the manuscript.

References and Notes

1. C. D. Mobley, *Light and Water: Radiative Transfer in Natural Waters* (Academic, San Diego, Calif. 1994).
2. R. W. Preisendorfer, "Application of radiative transfer theory to light measurements in the sea," Mongr. Intl. Union Geod. Geophys. Paris **10,** 11–30 (1961).
3. H. R. Gordon and W. R. McCluney, "Estimation of the depth of sun light penetration in the sea for remote sensing," Appl. Opt. **14,** 413–416 (1975).
4. H. R. Gordon, "Can the Lambert–Beer law be applied to the diffuse attenuation coefficient of ocean water," Limnol. Oceanogr. **34,** 1389–1409 (1989).
5. H. R. Gordon, "Dependence of diffuse reflectance of natural waters on the Sun angle," Limnol. Oceanogr. **34,** 1484–1489 (1989).
6. J. T. O. Kirk, "Monte Carlo study of the nature of the underwater light field in, and the relationships between optical properties of, turbid yellow waters," Aust. J. Mar. Freshwater Res. **32,** 517–532 (1981).
7. J. T. O. Kirk, "Dependence of relationship between inherent and apparent optical properties of water on solar altitude," Limnol. Oceanogr. **29,** 350–356 (1984).
8. J. T. O. Kirk, "Volume scattering function, average cosines, and the underwater light field," Limnol. Oceanogr. **36,** 455–467 (1991).
9. T. J. Petzold, "Volume scattering functions for selected natural waters," Scripps Inst. Oceanogr. Contrib. 72–78 (Scripps Institution of Oceanography, San Diego, Calif, 1972).
10. A. Morel and L. Prieur, "Analysis of variations in ocean color," Limnol. Oceanogr. **22,** 709–722 (1977).
11. G. H. R. and A. Y. Morel, *Remote Assessment of Ocean Color for Interpretation of Satellite Visible Imagery: a Review* (Springer-Verlag, New York 1983), p. 114.
12. A. Morel and B. Gentili, "Diffuse reflectance of oceanic waters: its dependence on Sun angles as influenced by the molecular scattering contribution," Appl. Opt. **30,** 4427–4438 (1991).

13. A. Morel and B. Gentili, "Diffuse reflectance of oceanic waters: bidirectional aspects," Appl. Opt. **32,** 6864–6879 (1993).
14. S. Sugihara, M. Kishino, and N. Okami, "Contribution of Raman scattering to upward irradiance in the sea," J. Oceanogr. Soc. Jpn. **40,** 397–404 (1984).
15. V. I. Haltrin, G. W. Kattawar, and A. D. Weidemann, "Modeling of elastic and inelastic scattering effects in oceanic optics," in *Ocean Optics XIII*, S. G. Ackleson, ed. Proc. SPIE **2963,** 597–602 (1996).
16. C. D. Mobley, B. Gentili, H. R. Gordon, J. Zhonghai, G. W. Kattawar, A. Morel, P. Reinersman, K. Stamnes, and R. H. Stavn, "Comparison of numerical models for computing underwater light fields," Appl. Opt. **32,** 7484–7504 (1993).
17. L. Prieur and S. Sathyendranath, "An optical classification of coastal and oceanic waters based on the specific absorption curves of phytoplankton pigments, dissolved organic matter, and other particulate materials," Limnol. Oceanogr. **26,** 671–689 (1981).
18. A. Bricaud, A. Morel, and L. Prieur, "Absorption by dissolved organic matter of the sea (yellow substance) in the UV and visible domains," Limnol. Oceanogr. **26,** 43–53 (1981).
19. L. Elterman, "UV, visible, and IR attenuation for altitude to 50 km," Rep. AFCRL-68-0153 (U.S. Air Force Cambridge Research Laboratory, Bedford, Mass., 1968).
20. E. P. Shettle and R. W. Fenn, "Models for the aerosols of the lower atmosphere and the effects of humidity variations on their optical properties," environmental res. paper 675, AFGL-TR-79-0214 (U.S. Air Force Geophysics Laboratories, Hanscom Air Force Base, Mass., 1979).
21. C. Cox and W. Munk, "Some problems in optical oceanography," J. Mar. Res. **14,** 63–78 (1955).
22. L. Prieur and A. Morel, "Etude théorique du régime asymptotique: relation entre caractéristiques optiques et coefficient d'extinction relatif à la pénétration de la lumière du jour," Cah. Oceanogr. **23,** 35–47 (1971).
23. A. Morel and B. Gentili, "Diffuse reflectance of oceanic waters. III. Implication of bidirectionality for the remote sensing problem," Appl. Opt. **35,** 4850–4862 (1996).
24. The optical thicknesses for the aerosol assemblages considered for the present computations and in Figs. 8 and 9 are 0.230, 0.222, 0.211, 0.198, 0.182 for λ = 410, 443, 490, 560, 665 nm, respectively, when $\tau_a(550) = 0.2$. When $\tau_a(550) = 0.4$ or $\tau_a(550) = 0.8$ the corresponding $\tau_a(\lambda)$ values are 0.444, 0.433, 0.417, 0.397, and 0.374 or 0.871, 0.853, 0.828, 0.796, and 0.758, respectively.
25. J. H. Ryther, "Photosynthesis and fish production in the sea," Science **166,** 72–76 (1969).
26. D. Antoine, J. M. André, and A. Morel, "Ocean primary production. 2. Estimation at global scale from satellite (coastal zone color scanner) chlorophyll," Global Biogeochem. Cycles **10,** 57–69 (1996).
27. R. C. Smith and K. S. Baker, "The bio-optical state of ocean waters and remote sensing," Limnol. Oceanogr. **23,** 247–259 (1978).
28. H. R. Gordon, O. B. Brown, R. H. Evans, J. W. Brown, R. C. Smith, K. S. Baker, and D. K. Clark, "A semianalytic radiance model of ocean color," J. Geophys. Res. **93,** 10,909–10,924 (1988).
29. A. Morel, "Optical modeling of the upper ocean in relation to its biogenous matter content (case 1 waters)," J. Geophys. Res. **93,** 10,749–10,768 (1988).